TTU-ES-70-2

A DYNAMIC POLARISCOPE FOR STRESS WAVE ANALYSIS

by

RAY KINSLOW

Prepared For

NATIONAL AERONAUTICS AND SPACE ADMINISTRATION

MANNED SPACECRAFT CENTER

HOUSTON, TEXAS

GRANT NUMBER NGR 43-003-007

JULY, 1970

TENNESSEE TECHNOLOGICAL UNIVERSITY

DEPARTMENT OF ENGINEERING SCIENCE

COOKEVILLE, TENNESSEE 38501

TTU-ES-70-2

A DYNAMIC POLARISCOPE FOR STRESS WAVE ANALYSIS

by

Ray Kinslow

Prepared For

NATIONAL AERONAUTICS AND SPACE ADMINISTRATION

MANNED SPACECRAFT CENTER

HOUSTON, TEXAS

GRANT NUMBER NGR 43-003-007

July, 1970

TENNESSEE TECHNOLOGICAL UNIVERSITY

DEPARTMENT OF ENGINEERING SCIENCE

COOKEVILLE, TENNESSEE 38501

ABSTRACT

A polariscope for the study of the propagation of stress waves in birefringent sheets is described. Very sensitive, fast-responding photomultiplier tubes, a laser light source, and a multiple channel oscilloscope were used for the simultaneous recording of the stress-optic data at several points of the target following impact. A method of separation of stresses and the computation of displacement, strain, and stress is given.

CONTENTS

ILLUSTRATIONS

Figure

A DYNAMIC POLARISCOPE FOR STRESS WAVE ANALYSIS

Introduction. Dynamic photoelasticity has been found to be an extremely useful tool for the study of stress wave propagation. Various experimental methods have been developed to record the photoelastic fringes resulting from impact or explosions. The use of the drum camera was introduced in 1936, followed by the microflash in 1946, the multiple spark camera in 1955, and the Q-spoiled ruby laser as a light source in 1966. High speed framing cameras and image converter cameras have been employed by many investigators.

One frame of a series of photographs made with a framing camera is shown in Figure 1. As the sheet of birefringent material was in a light-field polariscope, the half-order fringes are shown. From such photographs, the fringe order can be plotted as a function of position and the wave characteristics can be determined.

If a narrow beam of monochromatic light passing through a point of such a model is monitored by a fast responding light sensor, an oscilloscope record of the time-dependent fringes can be obtained. Clark (1) was apparently the first to report the recording of propagating stress fringes by this method. The work of other investigators using this method of studying stress waves are given in references (2) through (7).

A low-power Helium-Neon gas laser is an ideal light source as it provides a very narrow beam of monochromatic (6328 Å) light. The light sensor usually employed is a photomultiplier tube which, when connected to a high-frequency oscilloscope makes an excellent fringe counting

system. The cost of such a system is much less than the cost of a high-speed camera and intense light source.

There is, however, one great disadvantage to such a system. The optical output is nondiscriminating. Not only are the fringe values absolute, detecting no changes in the sign of the stress, but one cannot be certain of the fringe order by simply counting the peaks on the oscillogram as there is no direct way of determining whether the fringe order is increasing, decreasing, or remaining constant. This limitation is illustrated in Figure 2. A photomultiplier response is shown at the top of the figure. The first peak gives the time of the first half-order fringe (N = 0.5); and as this is a pressure wave, it is known to represent compression. It is assumed that the next peak represents a fringe order of three-halves (N = 1.5), but there is a possiblity that it may have a value of one-half also. As we progress across the record, it is seen that there are more than a thousand possible curves (1024 to be exact), only one of which represents the correct fringe order as a function of time. Many of the possibilities may be eliminated by simply saying that they do not look like stress waves. But are we ever sure? One would expect the two peaks representing the maximum fringe order to be spaced either closer together or farther apart than the adjacent ones. On this basis, it is believed that the fifth and sixth peaks on the oscillogram indicate the times of the maximum fringe order of nine halves (N = 4.5), and the curve drawn with the heavier line is the correct one. This clue, however, may not always be present.

Investigators using the laser-photomultiplier system generally employ some other means to verify and supplement the data. Okada, Cunningham, and Goldsmith (4) did this by taking fringe photographs.

They also fastened strain gages to the surface of the model near the point being monitored and recorded the strain gage data simultaneously with the photomultiplier output. Cunningham, Brown, and Griffin (6), and Bradley and Kobayashi (7) also used strain gages to supplement their data. Such a simultaneous record is shown in Figure 3. The strain gage response shows the approximate location of the maximum stress so that an accurate fringe order curve can be drawn by simply projecting from the oscillograph. Bohler and Shumann (8) used the oblique incidence method to separate the principal stresses.

Experimental Methods and Apparatus. The target, a 12 x 12 inch sheet of 0.25 inch Hysol 4485, was placed between two sheets of circularly polarizing filters as shown in Figure 4. A 4-milliwatt Helium-Neon continuous gas laser served as the monochromatic light source. The light was directed to four points on the target located one inch apart by means of three bifurcated fiber light guides as shown. The light was collimated into beams 0.070 inch in diameter. The four points were in a line perpendicular to the target edge and in line with the projectile path. After passing through the target, the light was directed by fiber light guides to four photomultiplier tubes (RCA 931A), the outputs of which were connected to a Tektronix Type 3A74 four-trace amplifier plug-in Type 564 storage oscilloscope. To avoid damage to the target and to reduce the contact time of the projectile, a metallic protector was attached to the target with a thin film of wax. A miniature accelerometer of the piezoelectric compression type was attached to the protector to serve as the oscilloscope sweep trigger. Stress waves were generated by impacting the metal protector with 0.22 caliber lead pellets fired from a compressed air gun.

Records of the light retardations caused by the photoelastic stress fringes as detected by the photomultiplier tubes are shown in Figure 5. Those four points located at distances of 3, 4, 5, and 6 inches from the point of impact were recorded by the four-trace amplifier. The ones at 2 and 7 inches were made by shifting the model to two other positions and repeating the shots. Excellent records could be obtained by monitoring the stress wave at eight points and recording the response of eight photomultiplier tubes on two four-channel oscilloscopes. If this were done, it would be possible to use a slower sweep for the more distant points and a faster sweep for the points near the impact in order to more accurately count and locate the various fringes. For example, if a point was located closer than two inches to the impact, a faster sweep would be necessary to distinguish the first fringes and to determine their times accurately. Likewise, if points were located farther than seven inches, it would be necessary to use a slower sweep in order to obtain information on more than one or two fringes.

Analysis of Data. It has been pointed out that one would expect the two peaks of the oscillogram that represent the maximum (or minimum) fringe order to be spaced either closer together or farther apart than the adjacent ones. In Figure 5 it is obvious that the maximum fringe order is 4.5 at a distance of three inches from the point of impact, and at a distance of six inches the maximum fringe order is 1.5. One would strongly suspect the maximum to be 5.5 at a distance of two inches and 2.5 at five inches. In a group of four oscillograms there will probably be at least two or three that give this information. This can be confirmed by realizing that the peak of the stress wave moves

at a velocity approximately equal to that of the fringes. By employing this fringe counting technique, additional compensating schemes are unnecessary.

By carefully determining the time of each fringe from the oscillograms of Figure 5, the distance-time curve for each fringe can be plotted as shown in Figure 6. If any errors were made in the fringe number, they will be detected when these curves are drawn.

As the sheet of Hysol used for the target was twelve inches deep, the wave was reflected from the rear surface as shown. No points were plotted in the region of interaction of the reflected tensile wave with the pressure wave.

An analysis of the stress wave will be made for the time of two milliseconds. The intercepts of the several curves with the two millisecond line are carefully measured or projected as shown in Figure 7 to give the fringe order (N) as a function of position. This curve also represents the shear stress (τ) as the stress-optic relation is:

$$\tau = \frac{Nf}{2h}$$

where f is the material stress fringe value and h is the plate thickness, which in this case is 0.25 inches. Separation of the stresses is possible since the waves in this case propagate without rotation. Stresses are developed in both the direction of, and perpendicular to, the direction of wave propagation. Displacement occurs, however, only in the direction of wave motion. The displacements are specified by:

$$u_r = f(r) \quad , \quad u_\theta = 0$$

and the strain-displacement relations by

$$\epsilon_r = \frac{du_r}{dr} \quad , \quad \epsilon_\theta = \frac{u_r}{r}$$

The stress-strain equations are

$$\sigma_r = \frac{E}{1-\nu^2}\left[\epsilon_r + \nu\epsilon_\theta\right] \quad , \quad \sigma_\theta = \frac{E}{1-\nu^2}\left[\epsilon_\theta + \nu\epsilon_r\right]$$

and the shear stress has the value

$$\tau = \pm \frac{\sigma_\theta - \sigma_r}{2}$$

where E is Young's modulus and ν is Poisson's ratio.

From these relations

$$2\tau = \sigma_\theta - \sigma_r = \frac{E}{1+\nu}\left[\epsilon_\theta - \epsilon_r\right] = \frac{E}{1+\nu}\left[\frac{u_r}{r} - \frac{du_r}{dr}\right]$$

but

$$\frac{d}{dr}\left(\frac{u_r}{r}\right) = \frac{1}{r}\left[\frac{du_r}{dr} - \frac{u_r}{r}\right]$$

So

$$\sigma_\theta - \sigma_r = -\frac{E}{(1+\nu)}\left[r\frac{d}{dr}\left(\frac{u_r}{r}\right)\right]$$

$$\frac{d}{dr}\left(\frac{u_r}{r}\right) = -\frac{(1+\nu)}{E}\left(\frac{\sigma_\theta - \sigma_r}{r}\right)$$

$$\frac{u_r}{r} = -\frac{(1+\nu)}{E}\int\frac{\sigma_\theta - \sigma_r}{r}\,dr$$

$$\epsilon_\theta = \frac{u_r}{r} = \frac{2(1+\nu)}{E}\int\frac{\tau}{r}\,dr$$

$$\epsilon_r = \epsilon_\theta - \frac{2(1+\nu)}{E}\tau = -\frac{2(1+\nu)}{E}\left[\tau + \int\frac{\tau}{r}\,dr\right]$$

The radial and tangential stresses are, therefore,

$$\sigma_r = -\left(\frac{2}{1-\nu}\right)\left[\tau + (1+\nu)\int\frac{\tau}{r}\,dr\right]$$

$$\sigma_\theta = -\left(\frac{2}{1-\nu}\right)\left[\nu\tau + (1+\nu)\int\frac{\tau}{r}\,dr\right]$$

This derivation is essentially the same as described in Reference 9.

These relations may be stated in terms of the model material properties and the fringe order.

$$U_r = -\frac{(1+\nu)f}{Eh}\left[r\int\frac{N}{r}\,dr\right] = r\epsilon_\theta$$

$$\epsilon_r = -\frac{(1+\nu)f}{Eh}\left[N+\int\frac{N}{r}\,dr\right] = \frac{du}{dr}$$

$$\epsilon_\theta = -\frac{(1+\nu)f}{Eh}\left[\int\frac{N}{r}\,dr\right]$$

$$\sigma_r = -\frac{f}{h(1-\nu)}\left[N+(1+\nu)\int\frac{N}{r}\,dr\right]$$

$$\sigma_\theta = -\frac{f}{h(1-\nu)}\left[\nu N+(1+\nu)\int\frac{N}{r}\,dr\right]$$

Values of displacement, strain, and stress may now be determined by numerical integration.

As the purpose of this paper is to illustrate a method of stress wave analysis, the values will be computed in terms of E and f. Poisson's ratio is assumed to have a value of 0.38. The results are shown in Figures 8, 9, and 10.

Conclusion. The polariscope described in this paper provides an excellent low-cost method for the analysis of stress waves in birefringent materials. As this system detects the changes in light retardation, it is not affected by residual stress and time edge effects that may be present in the model. By the simultaneous monitoring of several points of waves that are propagating without rotation, it is possible to separate the principal stresses and to determine their individual values without introducing additional experimental data. By using polaroids imbedded in the model, this method may be expanded to the study of spherical stress waves resulting from high velocity impact.

REFERENCES

1. Clark, A. B. J., "Static and Dynamic Calibration of Photoelastic Model Material, CR-39," Proc. SESA, XIV(1), 195-204 (1957).

2. Meier, J. H., and Bogardus, F., "Dynamic Determination of Photoelastic Fringe Constant for Hysol 4290 Plastic," IBM Tech. Rept. TR.01.13.172662(1961).

3. Brown, G. W., and Selway, D. R., "Frequency Response of a Photoelastic Material," Proc. SESA, XXI(1), 57-63 (1964).

4. Okada, A., Cunningham, D. M., and Goldsmith, W., "Stress Waves in Pyramids by Photoelasticity," Experimental Mechanics, 8 (7), 289-299 (1968).

5. Duffy, J. and Lee, T. C., "Measurement of Surface Strain by Means of Bonded Birefringent Strips," Experimental Mechanics, 1 (9), 109-112 (1961).

6. Cunningham, D. M., Brown, G. W., and Griffith, J. C., "Photoelastometric Recording of Stress Waves," Engineering Mechanics, 10 (3), 114-119 (1970).

7. Bradley, W. B., and Kobayashi, A. S., "A Dynamic Photoelastic System," Office of Naval Research, NR 064 478, TR No. 9, 1969, AD 687162.

8. Bohler, P., and Schumann, W., "On the Complete Determination of Dynamic States of Stresses," Experimental Mechanics, 8 (3), 115-121 (1968).

9. Dally, J. W., and Riley, W. F., "Stress Wave Propagation in a Half-Plane Due to Transient Point Load," Developments in Theoretical and Applied Mechanics, Vol. 3, Pergamon Press, New York, 1967, pp. 357-377.

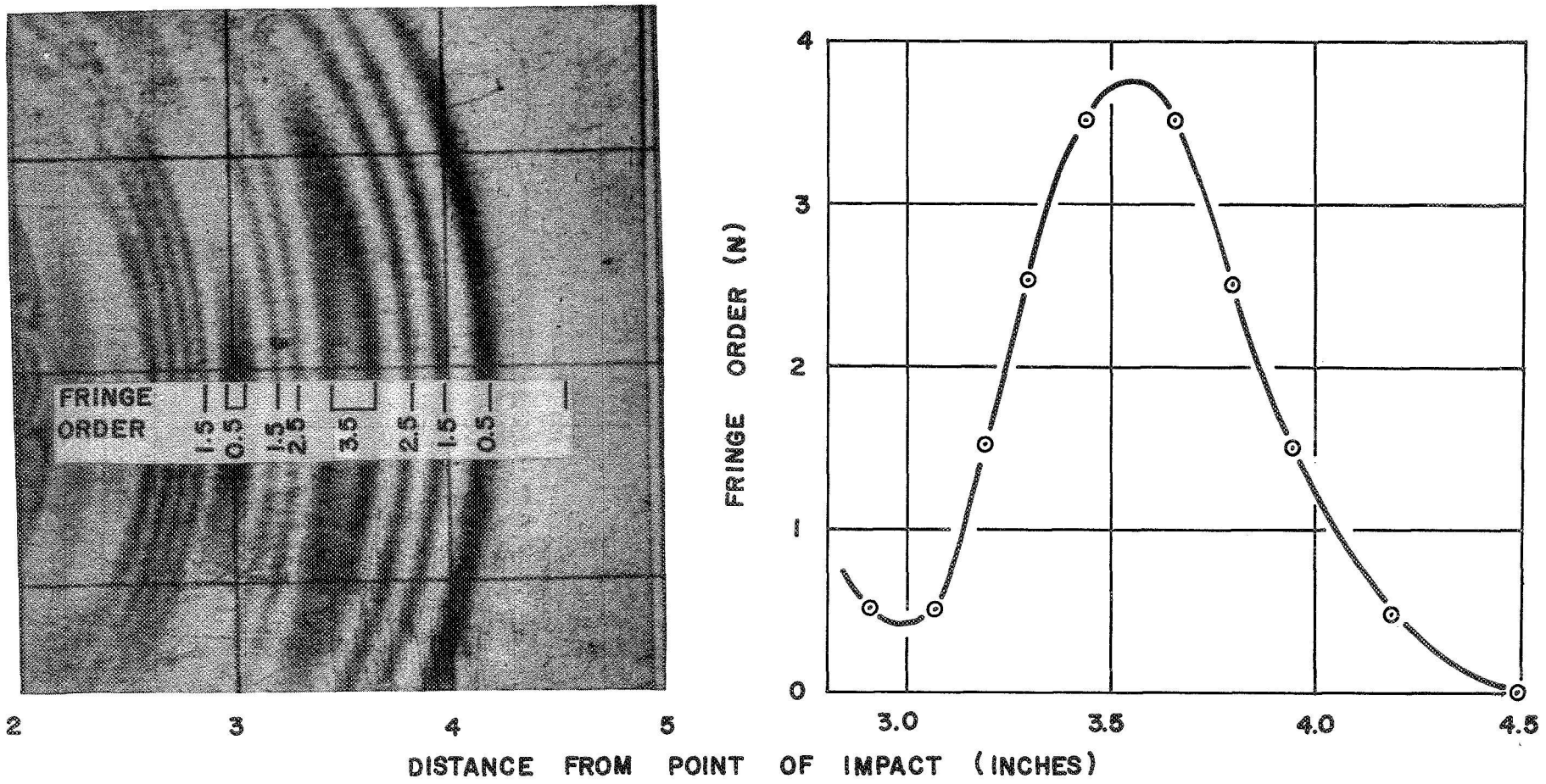

FIGURE I. FRINGE ORDER VERSUS POSITION AS DETERMINED FROM PHOTOGRAPH

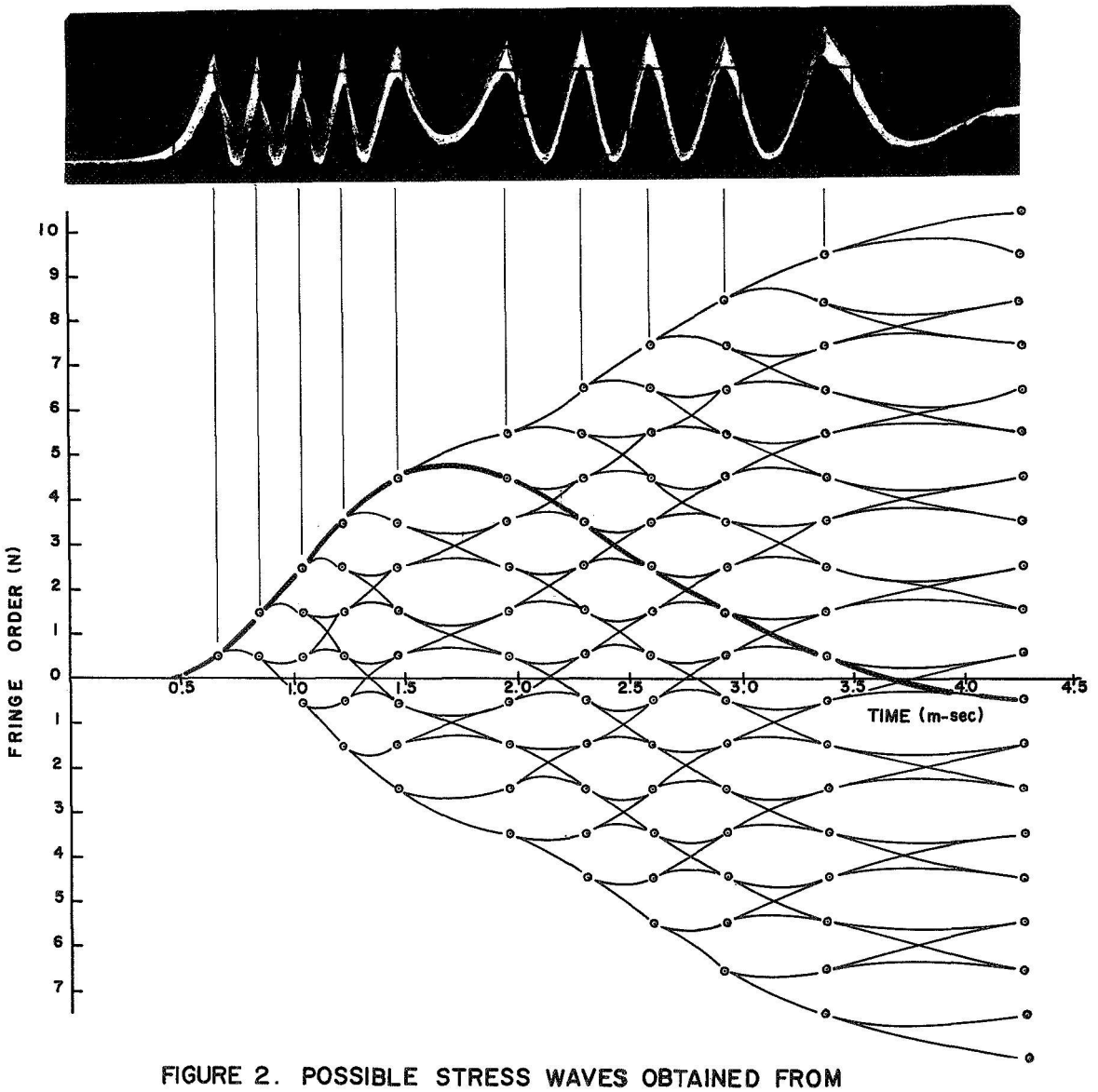

FIGURE 2. POSSIBLE STRESS WAVES OBTAINED FROM PHOTOMULTIPLIER TUBE RESPONSE

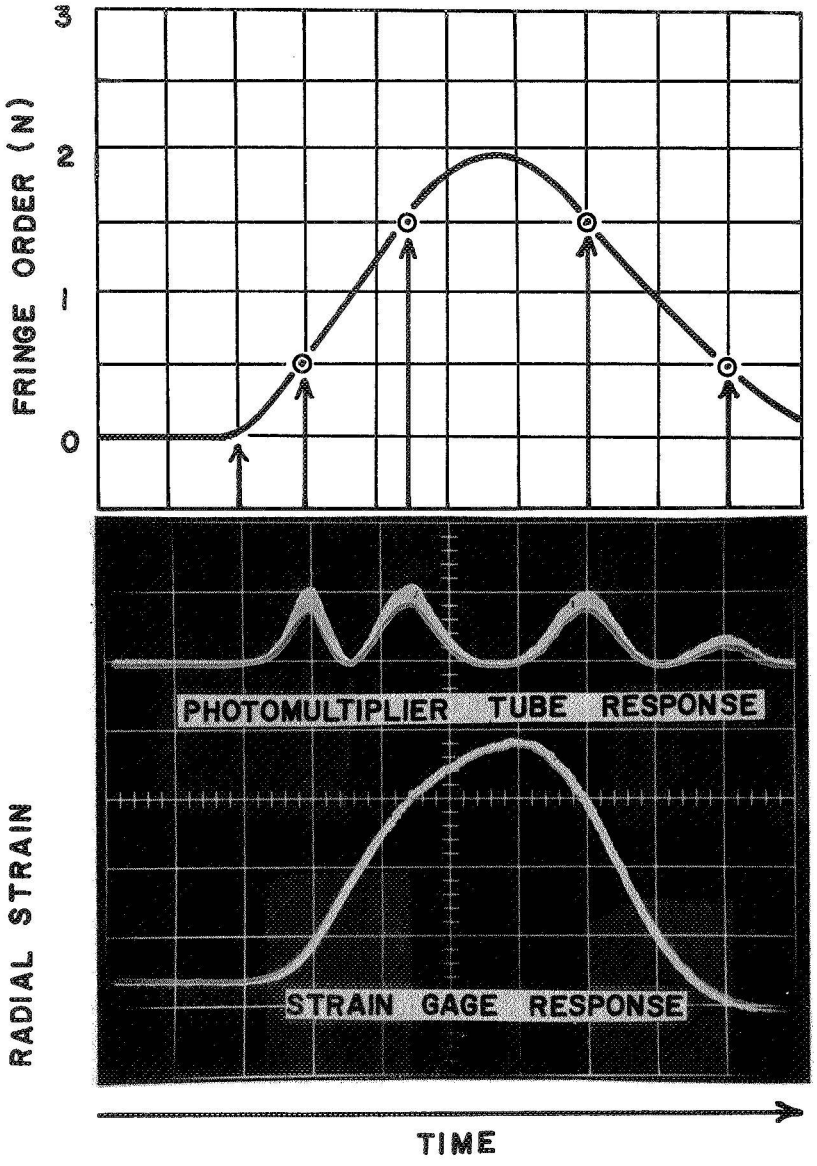

FIGURE 3. COMPARISON OF PHOTOMULTIPLIER TUBE AND STRAIN GAGE RESPONSE

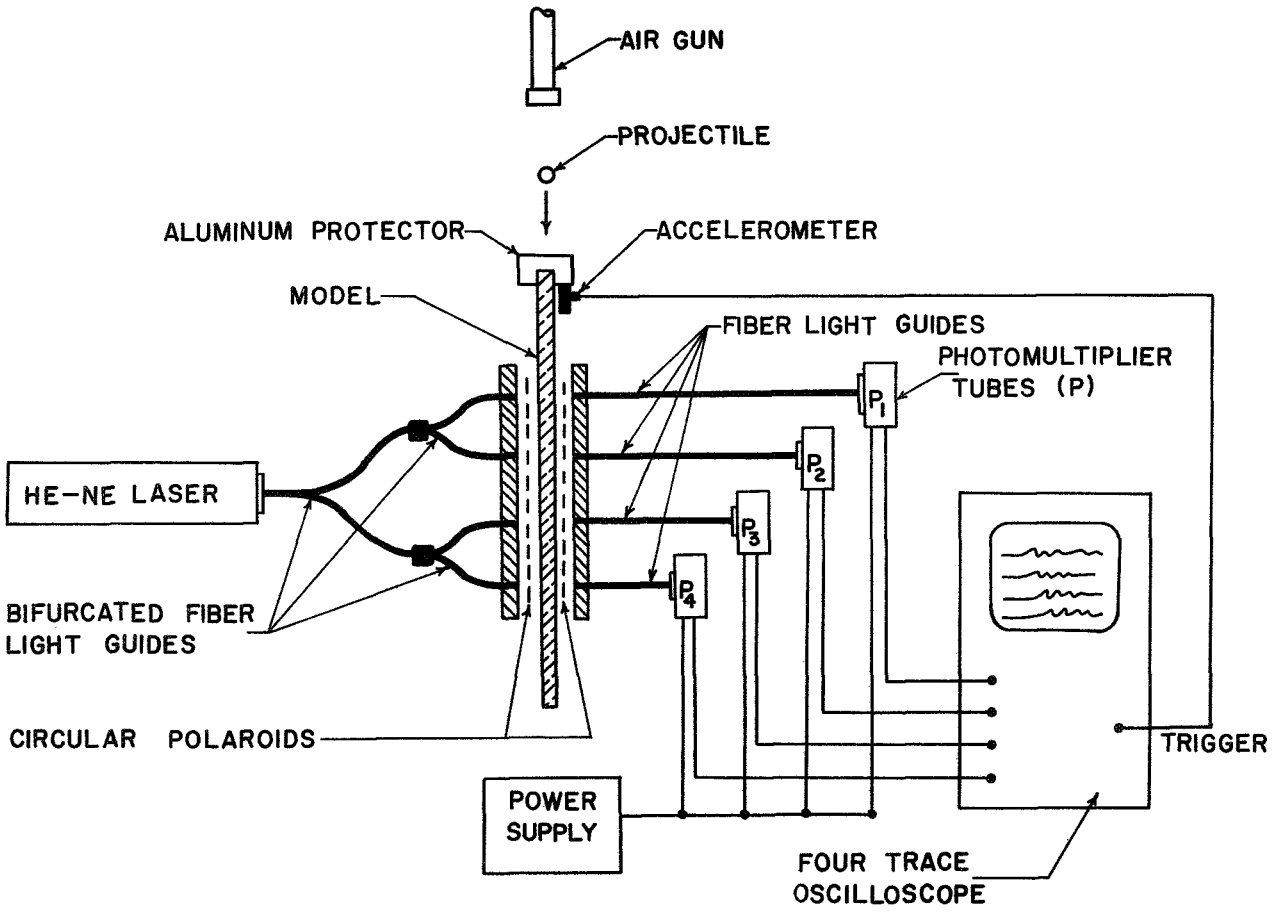

FIGURE 4. SCHEMATIC OF DYNAMIC POLARISCOPE

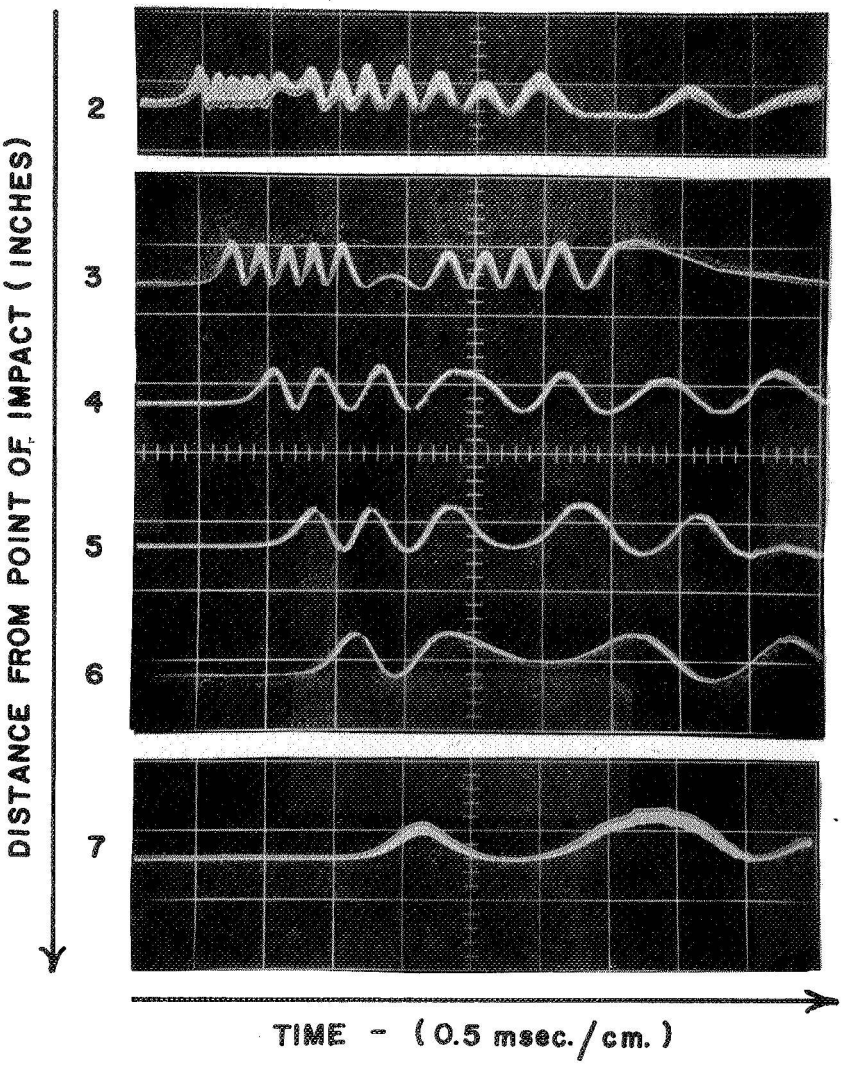

FIGURE 5. PHOTOMULTIPLIER TUBE RESPONSE AT VARIOUS DISTANCES FROM POINT OF IMPACT

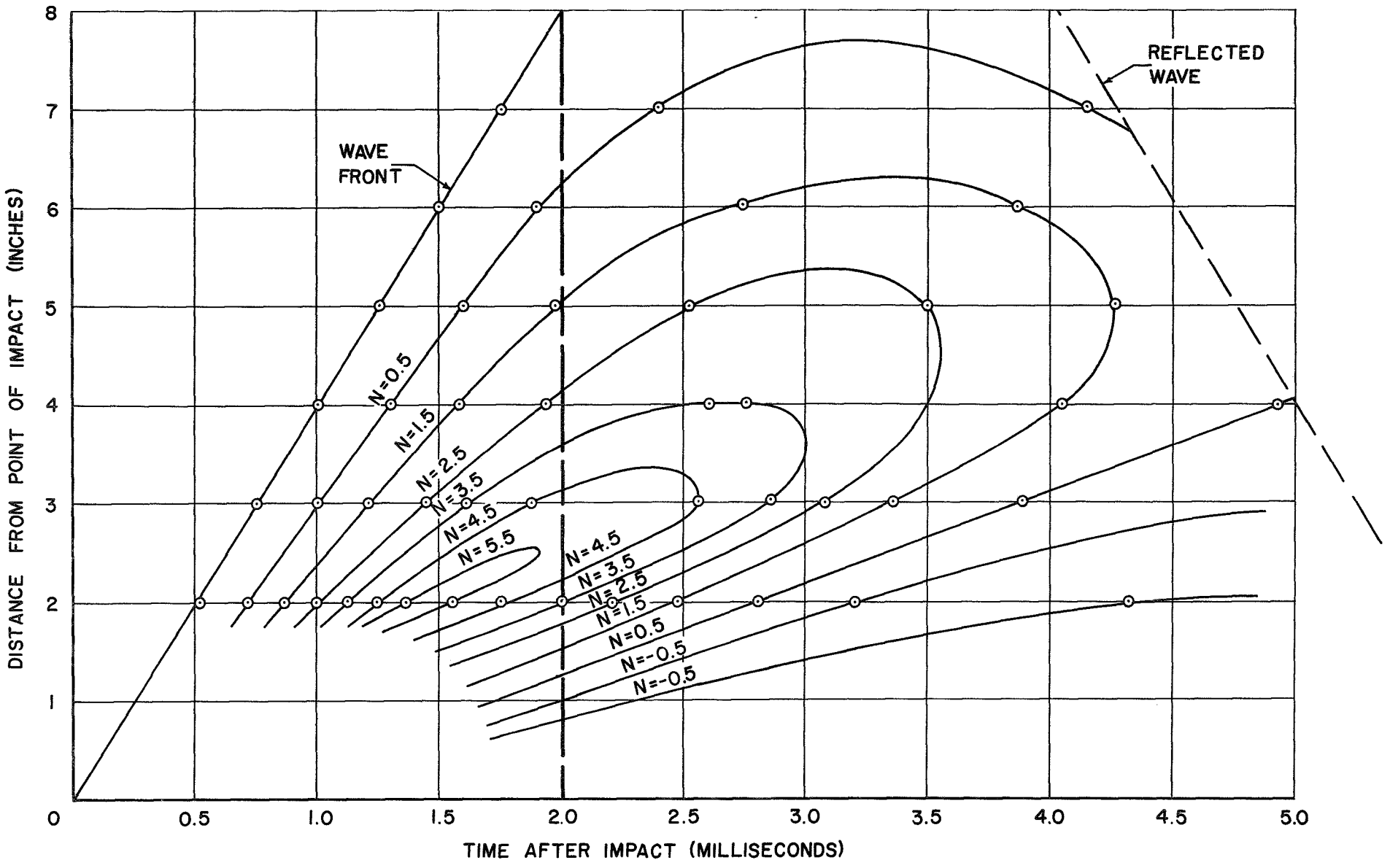

FIGURE 6. FRINGE - DISTANCE - TIME RELATION

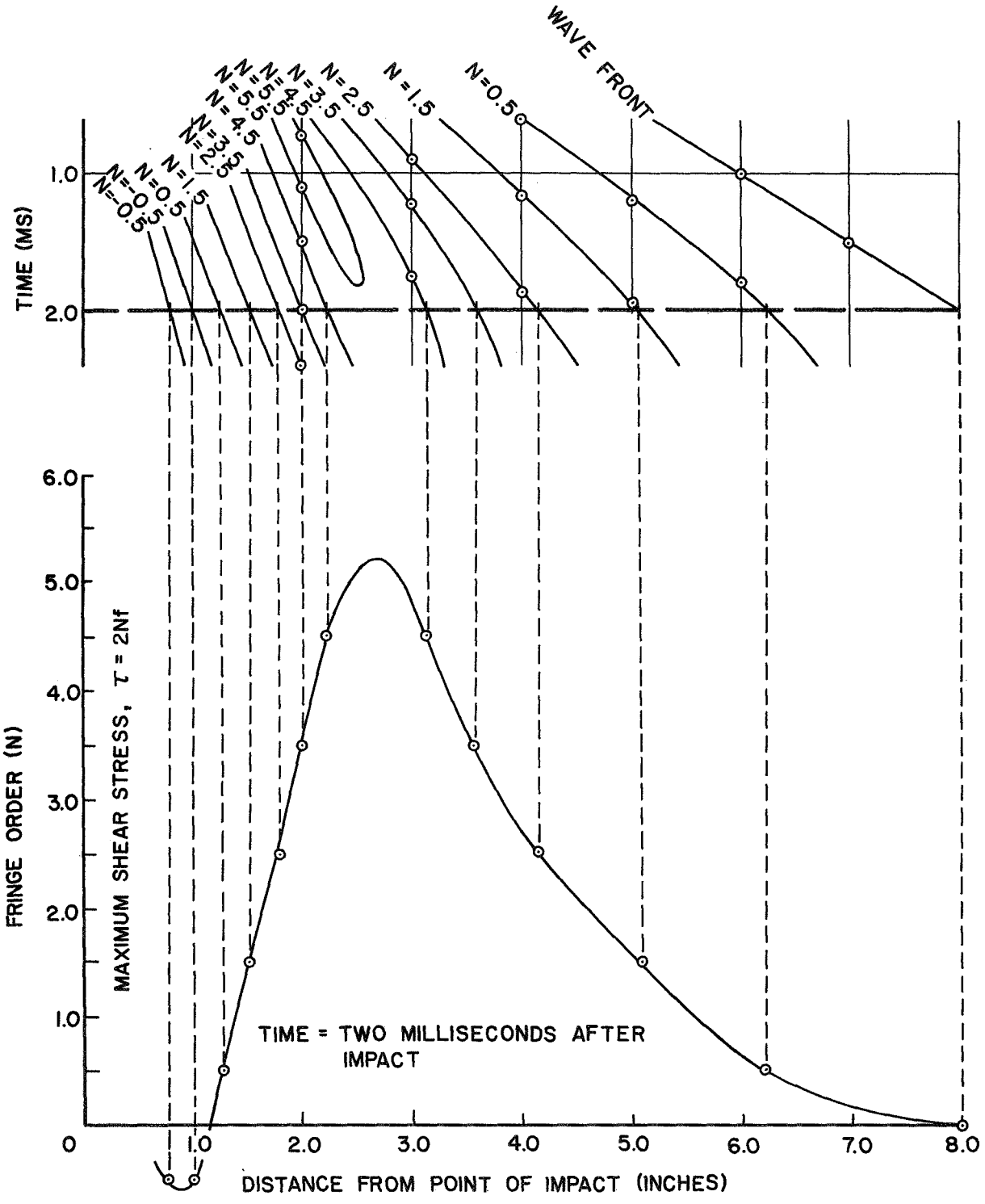

FIGURE 7. FRINGE ORDER AND SHEAR STRESS AS A FUNCTION OF POSITION

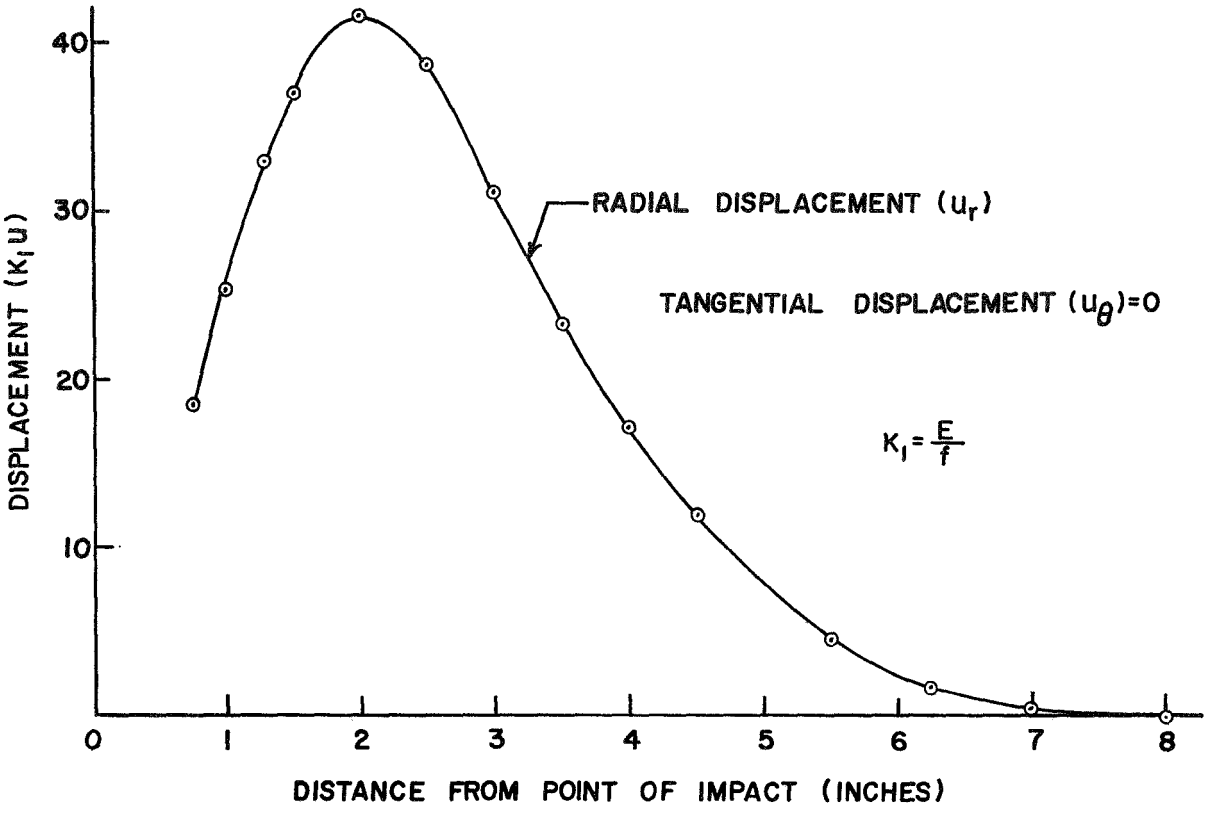

FIGURE 8. DISPLACEMENT

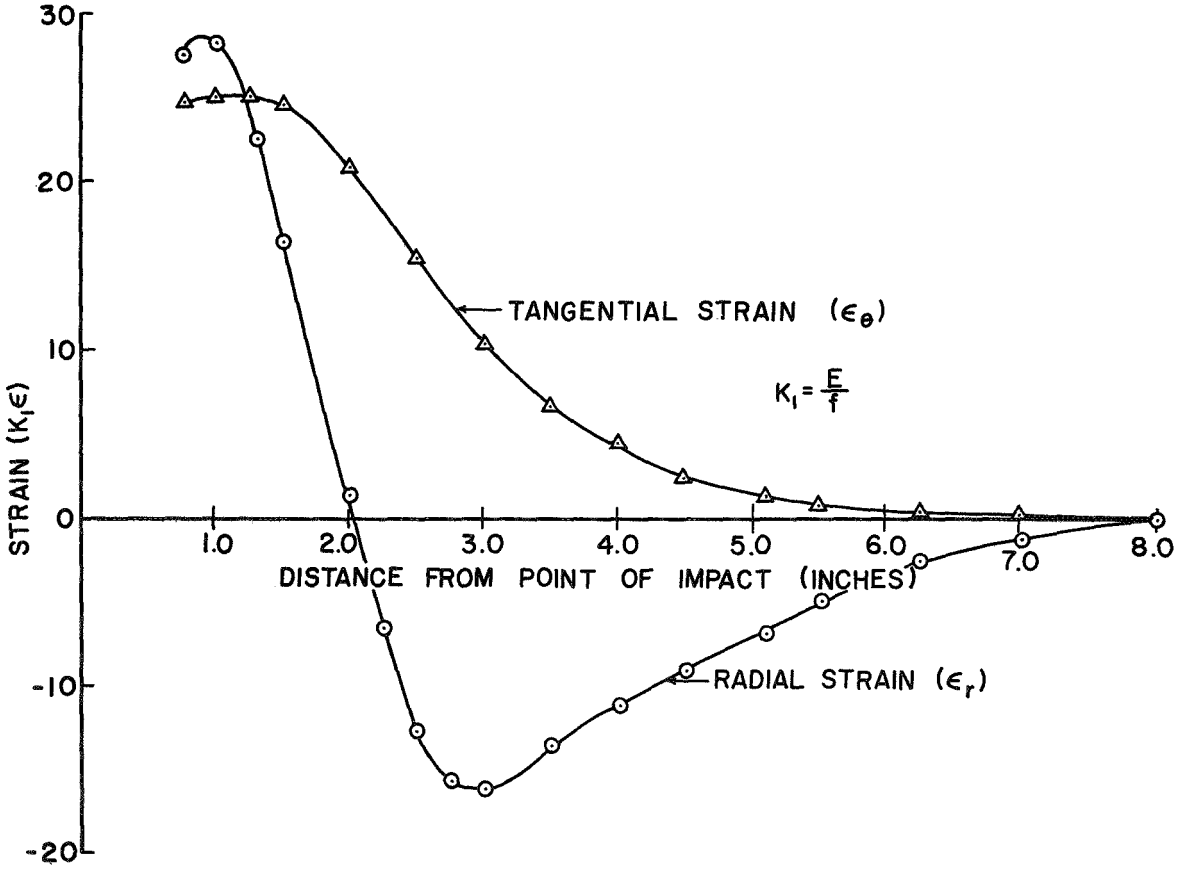

FIGURE 9. PRINCIPAL STRAINS

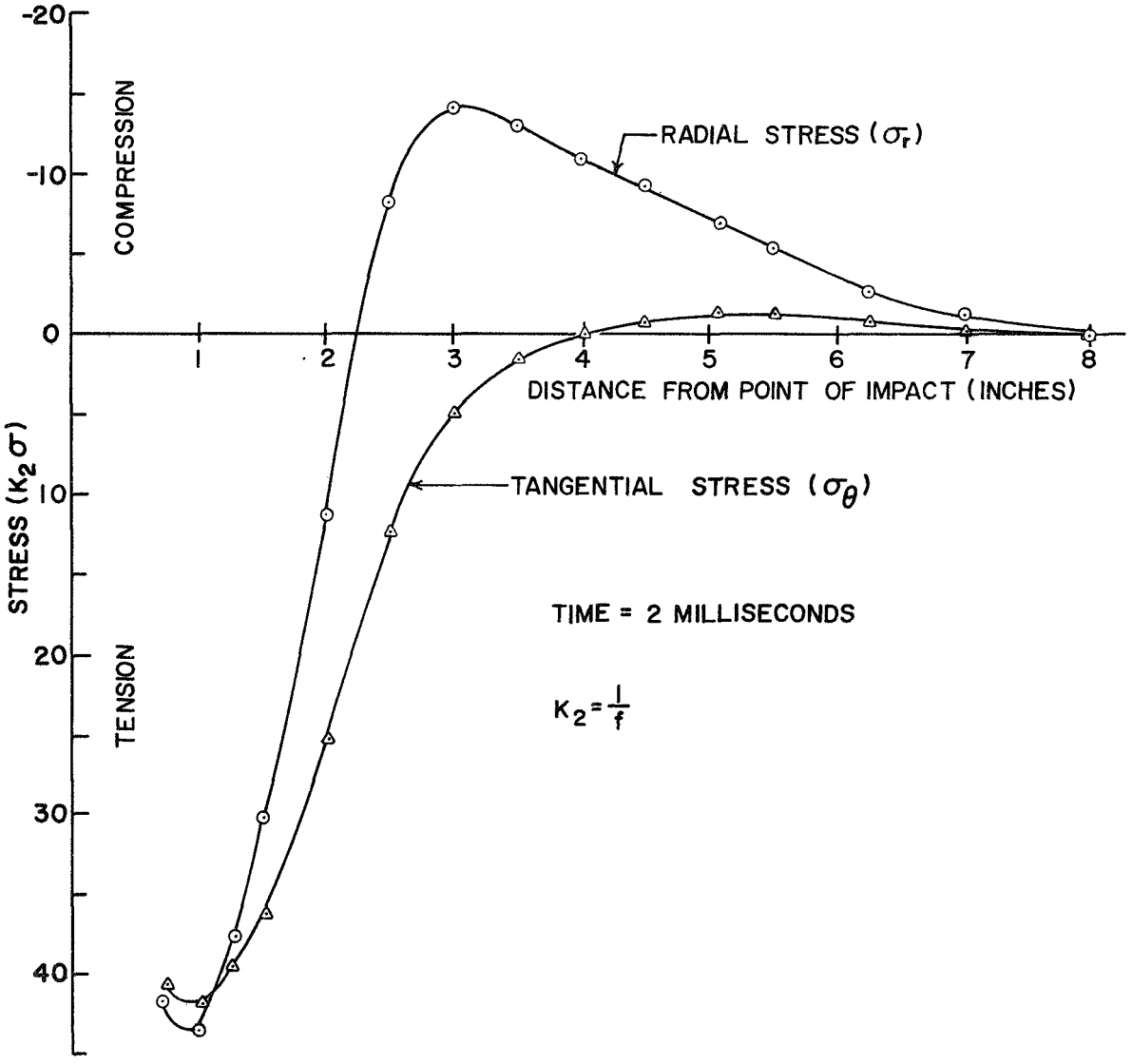

FIGURE 10. PRINCIPAL STRESSES